Research Article | Vol. 28, No. 2 / 20 January 2020 / Optics Express 1291
Optics EXPRESS

Curvature sensing with a D-shaped multicore fibre and Brillouin optical time-domain reflectometry

ANGELIKI ZAFEIROPOULOU,[1,2,4] ALI MASOUDI,[1,3] APOSTOLOS ZDAGKAS,[1] LAURENCE COOPER,[2] AND GILBERTO BRAMBILLA[1]

[1] *Optoelectronics Research Centre, University of Southampton, Southampton SO17 1BJ, United Kingdom*
[2] *Fibercore, Southampton Science Park, Fibercore House, University Parkway, Chilworth, Southampton SO16 7QQ, United Kingdom*
[3] *A.Masoudi@soton.ac.uk*
[4] *A.Zafeiropoulou@soton.ac.uk*

Abstract: A distributed curvature sensor based on Brillouin optical time-domain reflectometry interrogation technique in a D-shaped 7-core fibre is presented. By comparing the relative Brillouin frequency shift between the central core and three of the outer cores of the 7-core fibre, the curvature of various spools with different diameters is measured with a deviation from the actual value ranging between 9% and 15%. The analysis and results presented in this study show the first demonstration of distributed bend sensing using a specially designed multicore D-shaped fibre, paving the way for fully distributed 3D shape sensing.

1. Introduction

Curvature measurement is crucial for the Structural Health Monitoring (SHM) of bridges, cables [1], beams, slabs and domes [2] as it can give indications about the state of such structures. A local crack in a beam for instance, may result in a change in its curvature at the location of the crack. The changes in the curvature of a structure can also be used to calculate the deflection by integrating twice the curvature (which is a function of distance). This analysis is particularly interesting in SHM of arch dams with curved walls. Curvature measurement is possible with the use of optical fibre sensors which are offering many advantages over the conventional strain gauges such as small dimensions, robustness, ability to be used in inaccessible places, and immunity to external electromagnetic fields [3]. Multi-Core Fibres (MCFs) in particular, have attracted considerable attention over the last few years in sensing [4,5]. This is due to their intrinsic advantages, such as well-defined core separation and isothermal behaviour which follows from the fact that all cores are located within the same cladding.

Fibre Bragg Gratings (FBGs) have been widely explored for strain and curvature sensing. Davis et al. used wavelength division multiplexing to monitor strain at multiple points along an optical fibre which was attached to a cantilever beam [6]. The deformation of the beam was calculated based on the strain measurements from three FBGs placed at different locations along the beam. This sensor relied on an array of FBGs written in a single core fibre to form a quasi-distributed bend sensor. In 1999, a rubber tape called ShapeTape™ [7] became the first commercial fibre-optic 3D measurement device based on surface pressure measurements. However, it proved extremely costly [3]. Directional bend sensing has also been investigated in the past using FBGs. The first bend sensor based on FBGs written in MCFs was reported in [8] where FBGs were inscribed simultaneously in two-cores of a 4-core fibre for uniaxial bend measurements. Araújo et al. [9] used three FBGs placed in the vertices of an equilateral triangle to simultaneously measure the curvature and the plane of curvature, opening the way for three-dimensional (3D) shape sensing. In 2003, the use of FBGs for biaxial curvature

#383096 https://doi.org/10.1364/OE.383096
Journal © 2020 Received 12 Nov 2019; revised 28 Dec 2019; accepted 28 Dec 2019; published 8 Jan 2020

Optics EXPRESS

measurement was demonstrated by inscribing FBGs in three separate cores of a 4-core fibre [4]. The use of FBGs for sensing offers the advantage of a high spatial resolution, typically in the range of a few cm. However, the sensing range and the spatial resolution are limited by the finite number of FBGs inscribed in the fibre.

In the work reported in [10], continuous 3D shape monitoring was achieved using a 3-core fibre in an Optical Frequency-Domain Reflectometry (OFDR) interrogation setup. Shape sensing based on the OFDR technique offers the advantage of high spatial resolution combined with continuous measurements as oposed to FBGs which offer a quasi-distributed alternative. However, a reference measurement is always required for calibration purposes [11] which turns out to be impractical in case of long sensing systems.

Szostkiewicz et al. have also demonstrated a distributed curvature sensor based on phase-sensitive Optical Time-Domain Reflectometry (ϕ-OTDR) [12]. However, like the OFDR-based distributed shape sensors, this technique also requires a reference measurement with a straight fibre since it is not capable of measuring the absolute strain-level.

The capability of performing curvature measurements using Brillouin scattering was explored by Zhao et al. [5] using Brillouin Optical Time-Domain Analysis (BOTDA). In that work, a range of curvatures between $10\,\mathrm{m}^{-1}$ to $35\,\mathrm{m}^{-1}$ were measured with a spatial resolution of 20 cm and an error smaller than 8% over a 1 km long fibre. Although BOTDA is a powerful technique for long range sensing, it requires access to both ends of the fibre. In addition, BOTDA is best reserved for monitoring an abrupt change in the curvature where the strain-induced Brillouin frequency shift relative to the straight fibre is greater than the Brillouin linewidth.

In this study, Brillouin Optical Time-Domain Reflectometry (BOTDR) is used for distributed curvature measurement. In contrast to BOTDA, this approach requires a simpler interrogation setup and access to only one end of the sensing fibre. In addition, the fibre twist, which distorts the 3D coordinate system needed for the accurate determination of the curvature of a structure, is eliminated by the use of a specialty optical fibre, with D-geometry. The proposed geometry, which forces the fibre to bend preferentially, offers the advantage of avoiding the tedious task of manually maintaining the fibre orientation, paving the way for long range, distributed, shape sensing applications in the field.

2. Principle of operation

The operation of the sensor is based on measuring the strain-induced Brillouin Frequency Shift (BFS) in different cores of a MCF. As the fibre bends, different cores of the MCF experience different strain levels. By measuring the BFS in different cores, the curvature can be calculated. In this section, the impact of bending on the BFS of different cores of a 7-Core Fibre (7CF) is analyzed and the equation that determines the curvature of the fibre is derived [13].

For the fibre cross-section shown in Fig. 1(a), continuum mechanics shows that the material located farther from the neutral axis is under tension, while the material below the neutral axis is under compression. Using the strain-curvature relationship, the radius of curvature is given by,

$$R = \frac{r_2}{\epsilon_{2,4}} = \frac{r_7}{\epsilon_{7,4}} \tag{1}$$

$$R = \frac{r_2}{\epsilon_{2,4}} = \frac{r_3}{\epsilon_{3,4}}, \tag{2}$$

where R is the radius of curvature, r_2, r_3, r_7 are the distances of the cores $2, 3, 7$ from the neutral axis, respectively and $\epsilon_{2,4}, \epsilon_{3,4}, \epsilon_{7,4}$ are the difference in the strain values between cores $2, 3, 7$ and the central core (core 4), respectively. From Fig. 1(a), it can be shown that:

$$r_2 = r \cdot \sin\theta_2 = r \cdot \sin\left(\theta_7 + \frac{2\pi}{3}\right) \tag{3}$$

Optics EXPRESS

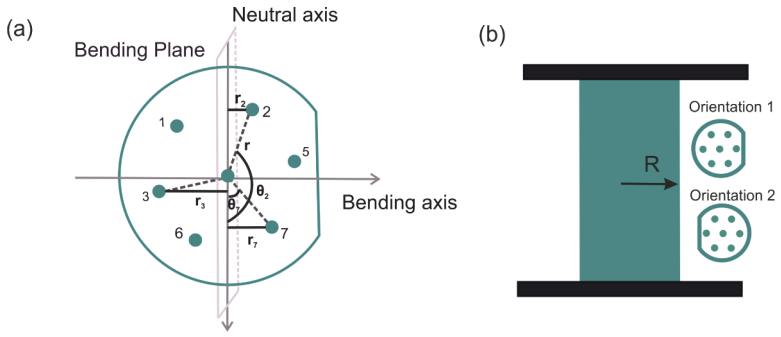

Fig. 1. (a) Coordinate system and cores' arrangement relative to the neutral axis. (b) Preferential bending of the D-shaped 7CF around the bobbin. The bending plane is parallel to the flat side of the fibre.

$$r_3 = r \cdot \sin\theta_3 = r \cdot \sin\left(\theta_2 + \frac{2\pi}{3}\right) \tag{4}$$

$$r_7 = r \cdot \sin\theta_7, \tag{5}$$

where r is the 7CF core pitch and $\theta_2, \theta_3, \theta_7$ are the angles between cores 2, 3, 7 and the neutral axis, respectively. By substituting Eqs. (3), (4) and (5) into Eqs. (1) and (2) and using some mathematical manipulation, it can be shown that:

$$\theta_2 = \cot^{-1}\left(\frac{\frac{\epsilon_{3,4}}{\epsilon_{2,4}} - \cos\left(\frac{2\pi}{3}\right)}{\sin\left(\frac{2\pi}{3}\right)}\right) \tag{6}$$

$$\theta_7 = \cot^{-1}\left(\frac{\frac{\epsilon_{2,4}}{\epsilon_{7,4}} - \cos\left(\frac{2\pi}{3}\right)}{\sin\left(\frac{2\pi}{3}\right)}\right). \tag{7}$$

In these equations, the values of $\epsilon_{2,4}$, $\epsilon_{3,4}$, and $\epsilon_{7,4}$ are determined by measuring the BFS using a BOTDR setup and the strain information is then used to determine the values of θ_2 and θ_7. By replacing the value of θ_2 and θ_7 in Eq. (4) and (3) the values of r_3, r_2 can be calculated. Finally, by substituting these values in Eq. (1) and Eq. (2), the radius of curvature is determined.

Although the asymmetric geometry of the D-shaped fibre suggests that the opposite cores of a bent 7CF experience slightly different strain levels, Finite Element Analysis (FEA) of the strain distribution over the fibre cross-section showed that this difference is negligible. Hence, to simplify the mathematical analysis, it is assumed that the opposite cores within the 7CF experience similar strain levels with opposite signs.

A common obstacle when attempting to do shape sensing using multicore optical fibres, is the random twist of the fibre that is introduced when the fibre is wrapped around the structure of interest. This twist can distort the 3-axes coordinate system needed for shape or curvature sensing which subsequently results in a large error in the determination of the curvature. In the work by Zhao et al. [5], an optical microscope was used to manually orient the fibre and maintain the relative position of the cores with respect to the bending plane. However, this approach might be impractical as it cannot be easily implemented in the field. In this work, a multicore fibre with a D-shape geometry is proposed as a way to achieve preferential bending. A fibre with said geometry is expected to bend preferentially along a certain direction due to its asymmetry, based on the fact that it is thinner along the axis where the milled side is and the associated moment of inertia is minimum. As a result, the energy required for compression and stretching of the fibre

Optics EXPRESS

along this preferential axis is minimized, forcing the fibre to always bend along a plane which is parallel to the flat side, as it appears in Fig. 1(b).

3. Experimental arrangement

3.1. Experimental setup

Figure 2 shows a schematic diagram of the experimental setup. Light from a Tunable Laser Source (TLS) at 1533 nm was amplified by an Erbium-Doped Amplifier (EDFA 1) and then split by a 70/30 coupler. Light from the 70% arm of the coupler was amplitude-modulated using an Electro-Optic Modulator (EOM) to generate a train of 20 ns pulses with a repetition rate of 1 MHz. The light was further amplified by another amplifier (EDFA 2) before entering an Acousto-Optic Modulator (AOM), which limits the Amplified Spontaneous Emission (ASE) entering the sensing fibre and it was synchronised with the EOM to allow the probe pulse to pass through.

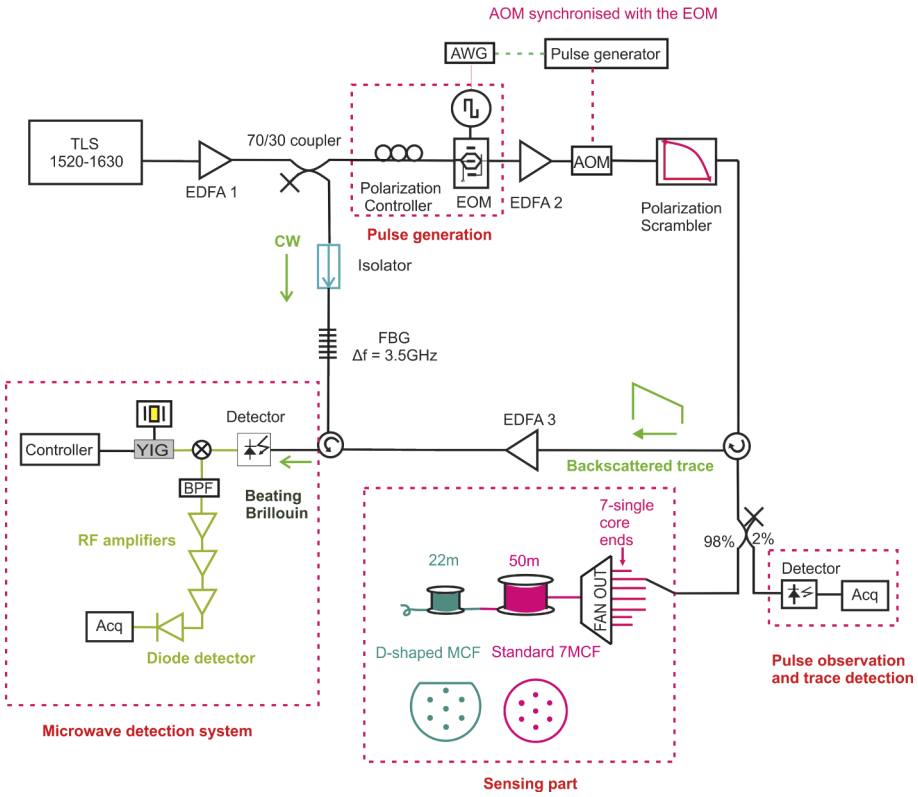

Fig. 2. Experimental Setup. TLS, Tunable Laser Source; AWG, Arbitrary Wave Function; EOM, Electro-Optic Modulator; EDFA, Erbium-Doped Fibre Amplifier; AOM, Acousto-Optic Modulator; BPF, Band Pass Filtre; YIG, Yttrium Iron Garnet synthesiser.

A polarisation scrambler was added in order to avoid polarisation fading. The amplified probe pulse with a peak power of 1 W was then launched into the sensing fibre via a circulator. A 98/2 tap coupler was added after the second port of the circulator to monitor the probe pulse. The remaining 98% of the power was sent to the sensing fibre via a fan-out demultiplexer. A 50 m length of standard 7CF was spliced to 22 m of D-shaped 7CF. The backscattered light from the sensing fibre was amplified by a third optical amplifier (EDFA 3) followed by a narrow bandwidth FBG (λ_B = 1533.35 nm, BW = 3.5 GHz) to separate the Brillouin anti-Stokes from

Optics EXPRESS

the Rayleigh backscattering. The Brillouin backscattered trace was mixed with the seed laser source and the generated beat signal, corresponding to the Brillouin frequency shift at around 11 GHz, was detected using a 15 GHz photodetector with a responsitivity greater than 0.65 A/W at 1300 nm. The frequency of the signal was further down-shifted using a microwave detection system. More specifically the backscattered signal from the sensing fibre was mixed with the signal generated by an Yttrium Iron Garnet (YIG) frequency synthesiser. After mixing, the signal was passed through a Band-Pass Filter (BPF) centred at 1 GHz , with a bandwidth of 50 MHz to generate an Intermediate Frequency (IF) of 1 GHz . The IF signal is amplified and then rectified using a microwave diode rectifier generating a signal proportional to the intensity of the Brillouin backscattering at the chosen frequency. An oven controlled crystal oscillator is used to provide the YIG synthesiser with a stable reference frequency.

3.2. Fabrication process of the D-shaped fibre

The D-shaped fibre preform was manufuctured by removing a portion of the cladding lengthwise in the circular optical fibre preform prior to drawing. The cores of the multicore D-shaped fibre were fabricated using the Modified Chemical Vapour Deposition (MCVD) technique. Holes were drilled into a F300 glass rod, which has high purity and a low OH content, and their surfaces were subsequently polished. The core preforms were fabricated with an extra large size and were then stretched and divided into 7 rods which were inserted into the preform holes. Vacuum was used during the holes sealing process in order to get a solid 7-core preform. As a final step of the preform fabrication, the 18 mm in diameter preform, was mounted on a milling bed and a diamond milling tool was used to mill one of its side by 1.6 mm. A temperature of 1900°C, 100°C lower than the standard drawing temperature was used, in order to maintain the "D" shape during the fibre drawing. The fibre was pulled with a tension of 160 g at a speed of 60 m/min. Figure 3 shows the geometry of the multicore fibre that was used as the sensing element. The fibre has a pitch of 35 μm and a core diameter of 5.3 μm.

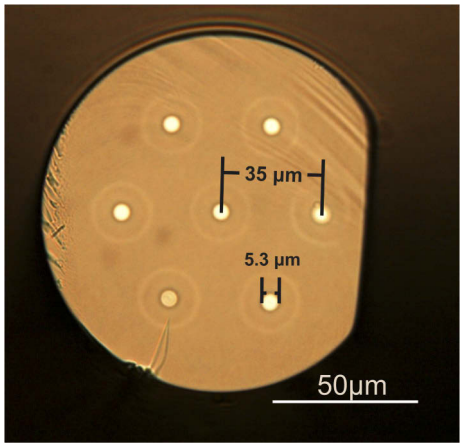

Fig. 3. Optical microscope image of the D-shaped fibre.

3.3. Experimental procedure

Four spools of different diameter (59 mm, 114 mm, 150 mm, 227 mm) were used for the curvature test. 22 m of the D-shaped fibre were wrapped around each of the spools using a rewinding machine and four different tests were carried out separately. The frequencies of the YIG synthesiser were scanned through a 300 MHz frequency range at 5 MHz steps using an Arduino controller. The

Optics EXPRESS

selected YIG frequency determined the Brillouin beat frequency that was measured: i.e. the measured component of the Brillouin spectrum was equal to the YIG frequency plus 1 GHz (the IF). The signal was fed to a storage oscilloscope with a sampling rate of 5 Gs/s, which was used to average 10,000 time-domain traces that were then transferred to the PC. The Brillouin spectra were built by collecting such traces over a range of frequencies determined by the YIG synthesizer [14]. The processes of scanning the frequencies, capturing the data and building the Brillouin gain spectra were automated using a MATLAB script. The automation reduces the time needed for a complete measurement and hence eliminates the introduction of errors due to temperature variations or drift of the electronic equipment.

4. Experimental results

Figure 4 shows the anti-Stokes Brillouin gain spectrum (BGS) of an outer core of a standard 7CF from 0 m to 60 m spliced to 22 m of D-shaped 7CF. As mentioned earlier, the D-shaped fibre shows a preferential bending direction with its neutral plane parallel to the flat side. This results in insignificant twist of the cores across the length. This phenomenon can be clearly seen in Fig. 4 where the BGS corresponding to the D-shaped fibre shows little deviation from its mean value compared with the BGS of the standard 7CF which exhibits notable fluctuations.

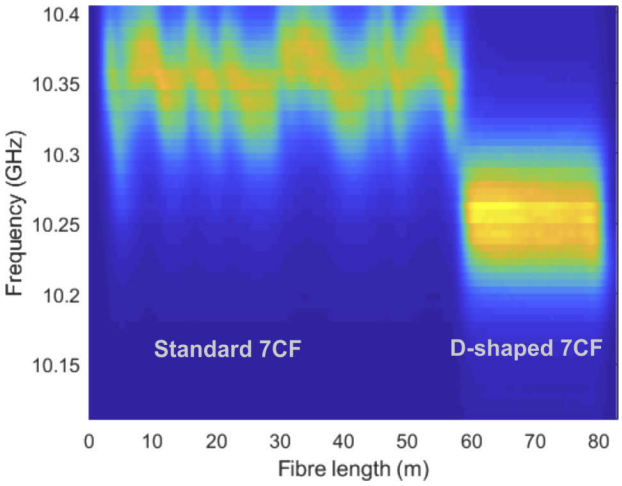

Fig. 4. BGS of an outer core of a standard 7-core fibre (0 m - 60 m) and of a D-shaped 7-core fibre (60 m - 80 m).

The horizontal and vertical axes of this diagram represent the distance along the sensing fibre and the BFS, respectively. This diagram was obtained by scanning the BGS over a frequency range of 300 MHz in 5 MHz steps. At each step, the backscattered traces were averaged 10,000 times to improve the Signal to Noise Ratio (SNR). Similar diagrams were created for each core of the three remaining bobbins and the BGS from different cores were used to calculate the radius of each bobbin.

5. Discussion

Figure 5 shows the fitted curves for the anti-Stokes BGS as a function of the frequency shift for six out of seven cores at the distance of 64.18 m of the D-shaped 7CF wrapped on a 114 mm diameter bobbin. It should be noted that the core closest to the milled side experiences high mode leakage losses and hence it is not taken into consideration for the curvature calculations.

Optics EXPRESS

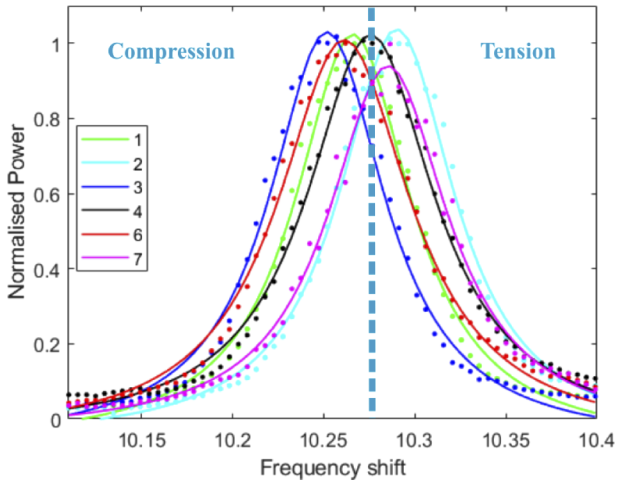

Fig. 5. BGS of a D-shaped fibre wrapped on a 114 mm spool at 64.18 m. Cores 1,3, and 6 are under compression relative to core 4 (central) while cores 2, and 7 are under tension.

The strain levels corresponding to opposite cores were compensated so as to be symmetrical around zero as shown in Fig. 6(a). More specifically, we expect the pair of cores 1 & 7, 2 & 6 and 3 & 5 to experience values of strain equal in amplitude but opposite in sign, since they are located in diametrically opposite sides within the fibre cladding, as shown in Fig. 1(a). However, in practice, the strain values of the opposite cores are not completely symmetric around zero. This is because, during the fabrication process, it is a standard practice to use preforms with slightly different refractive indices for the core material. To compensate for that, the mean strain value of a said core and the core opposite to it was subtracted from the strain value of the said core at a specific position. For instance,

$$\epsilon_1(\mathrm{x_i})_{\mathrm{comp}} = \epsilon_1(\mathrm{x_i}) - \epsilon_{\mathrm{mean}}(\mathrm{x_i}) \tag{8}$$

$$\epsilon_{\mathrm{mean}}(\mathrm{x_i}) = \left[\frac{\epsilon_1(\mathrm{x_i}) + \epsilon_7(\mathrm{x_i})}{2}\right], \tag{9}$$

where $\epsilon_{\mathrm{comp}}(\mathrm{x_i})$ represents the compensated strain of core 1 at position i. A similar procedure was followed for the pair of cores 2 & 6. However the strain values of core 3 were not compensated since the core positioned opposite to it, core 5, was experiencing high mode leakage due to its proximity to the flat side of the D-shaped fibre.

The bending radius at 64.18 m was calculated using three non-adjacent cores and Eq. (1)–(7). The BFS for each core, calculated by Lorentzian fits, were $f_1 = 10.2661$ GHz, $f_2 = 10.2901$ GHz, $f_3 = 10.2518$ GHz, $f_4 = 10.2757$ GHz, $f_6 = 10.2613$ GHz, and $f_7 = 10.2852$ GHz. Using the strain coefficient value of $0.046\,\mathrm{MHz}/\mu\epsilon$ [15] for all cores and the strain compensation method described above, the strain level of the cores were, $\epsilon_1 = -207.32\mu\epsilon$, $\epsilon_2 = 312.49\mu\epsilon$, $\epsilon_3 = -518.82\mu\epsilon$, $\epsilon_6 = -312.49\mu\epsilon$, and $\epsilon_7 = -207.32\mu\epsilon$. The strain values were replaced in Eq. (6)–(7) to determine $\theta_2 = -0.6412$, and $\theta_7 = 0.4073$. The values of θ were substituted in Eq. (3) - (5) to obtain $r_2 = 20.8987\mu$m, $r_3 = 34.7583\mu$m, and $r_7 = 13.8649\mu$m. The values of r_2, r_3, r_7 and ϵ_2, ϵ_3, ϵ_7 were replaced to Eq. (1), (2) to determine the radii of $\mathrm{R_2} = 6.6878$cm , $\mathrm{R_3} = -6.6995$cm , and $\mathrm{R_7} = 6.6878$cm . The mean radius of the three cores was subsequently calculated to determine the radius of the fibre at that point. This process was repeated for all the points along the sensing fibre. Finally, the mean bending radius along the length of the fibre as well as the standard deviation, were determined for that spool. The same process was repeated to determine the bending radii of the other three spools.

Optics EXPRESS

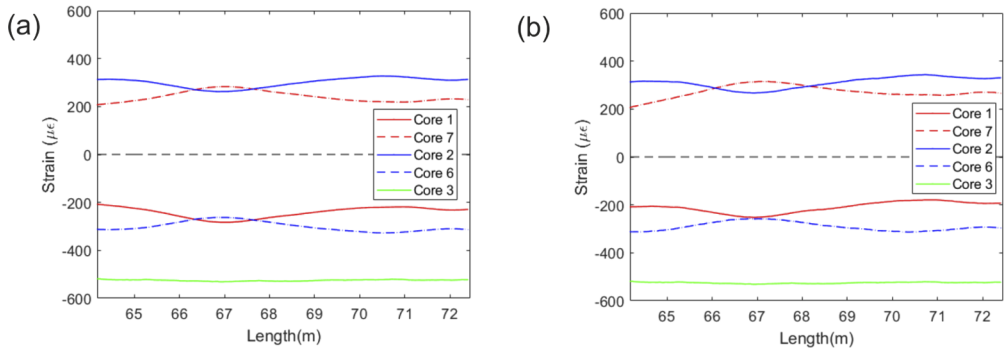

Fig. 6. Strain distribution as a function of length. Core 5 is not depicted due to the high mode leakage loss. (a) With compensation. (b) Without compensation.

Figure 7 shows the mean bending radius along the length of 2.5 m as well as their standard deviation for the four different spools used in this study, as a function of the actual bending radii. The blue curve depicts the ideal relation between the theoretical and the experimental values. The measurements match the expected linear behaviour.

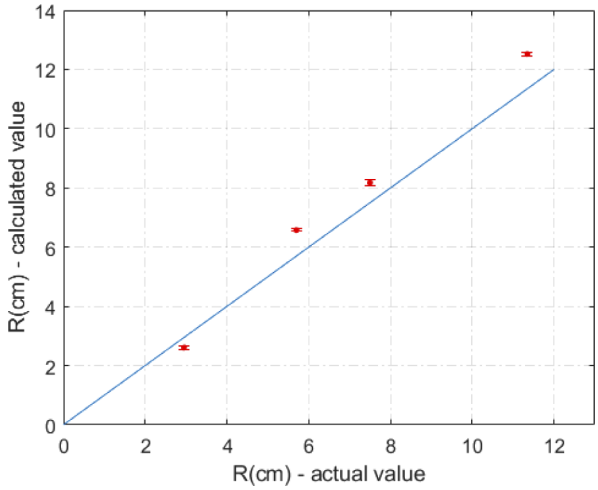

Fig. 7. Measured bending radius against the real bending radius.

A possible source of error is the noise originated from various components of the system such as the detector or the amplifiers. A drift in the laser intensity, as well as the temperature variation during the scanning of the frequencies which takes around 7 minutes, could also affect the accuracy in the determination of the bending radius. Lastly, a more precise determination of the Lorentzian fits can be achieved by reducing the step of scanning in the frequency domain. This requires a faster acquisition system which will be further investigated in a future work together with demonstrating fully 3D shape sensing abilities.

6. Conclusion

A fully distributed optical fibre bend sensor based on a multicore D-shaped fibre was demonstrated. BOTDR setup was used to measure diameters ranging from 59 mm to 227 mm with deviations between 9% and 15% depending on the diameter of the spool. The D-shaped geometry allows for

Optics EXPRESS

the preferential bending of the fibre with the flat side either on the inner or on the outer side of the bend, offering the advantage of self-orientating. In this way, the need to manually inspect the orientation of the cores is eliminated enabling its use to long-range applications. In combination with the single-ended access that BOTDR offers, the method presented in this work, is well suited for field applications.

Funding

H2020 Marie Skłodowska-Curie Actions (722509).

Acknowledgments

The author would like to thank Angeles Camacho Rosales for her help in taking the microscope image of the optical fibre.

Disclosures

The authors declare no conflicts of interest.

References

1. A. Masoudi, J. A. Pilgrim, T. P. Newson, and G. Brambilla, "Subsea cable condition monitoring with distributed optical fiber vibration sensor," J. Lightwave Technol. **37**(4), 1352–1358 (2019).
2. D. Inaudi, N. Casanova, and S. Vurpillot, "Bridge deformation monitoring with fiber optic sensors," in *International Association for Bridge and Structural Engineering (IABSE) Symposium*, (1999).
3. M. Amanzadeh, S. M. Aminossadati, M. S. Kizil, and A. D. Rakić, "Recent developments in fibre optic shape sensing," Measurement **128**, 119–137 (2018).
4. G. M. H. Flockhart, W. N. MacPherson, J. S. Barton, J. D. C. Jones, L. Zhang, and I. Bennion, "Two-axis bend measurement with Bragg gratings in multicore optical fiber," Opt. Lett. **28**(6), 387–389 (2003).
5. Z. Zhao, M. A. Soto, M. Tang, and L. Thévenaz, "Distributed shape sensing using Brillouin scattering in multi-core fibers," Opt. Express **24**(22), 25211–25223 (2016).
6. M. A. Davis, A. D. Kersey, J. Sirkis, and E. J. Friebele, "Shape and vibration mode sensing using a fiber optic bragg grating array," Smart Mater. Struct. **5**(6), 759–765 (1996).
7. R. Balakrishnan, G. W. Fitzmaurice, G. Kurtenbach, and K. Singh, "Exploring interactive curve and surface manipulation using a bend and twist sensitive input strip," in *Association for Computing Machinery (ACM) Symposium on Interactive 3D Graphics*, (1999).
8. M. J. Gander, W. N. MacPherson, R. McBride, J. D. C. Jones, L. Zhang, I. Bennion, P. M. Blanchard, J. G. Burnett, and A. H. Greenaway, "Bend measurement using Bragg gratings in multicore fibre," Electron. Lett. **36**(2), 120–121 (2000).
9. F. M. Araújo, L. A. Ferreira, and J. L. Santos, "Simultaneous determination of curvature, plane of curvature, and temperature by use of a miniaturized sensing head based on fiber Bragg gratings," Appl. Opt. **41**(13), 2401–2407 (2002).
10. R. G. Duncan, M. Froggatt, S. Kreger, R. Seeley, D. K. Gifford, A. K. Sang, and M. S. Wolfe, "High-accuracy fiber-optic shape sensing - art. no. 65301s," in *Proc. SPIE - The Int. Soc. for Opt. Eng.*, (2007).
11. A. Masoudi and T. P. Newson, "Contributed review: Distributed optical fibre dynamic strain sensing," Rev. Sci. Instrum. **87**(1), 011501 (2016).
12. Ł. Szostkiewicz, M. A. Soto, Z. Yang, A. Dominguez-Lopez, I. Parola, K. Markiewicz, A. Pytel, A. Kołakowska, M. Napierała, T. Nasiłowski, and L. Thevenaz, "High-resolution distributed shape sensing using phase-sensitive optical time-domain reflectometry and multicore fibers," Opt. Express **27**(15), 20763–20773 (2019).
13. J. P. Moore and M. D. Rogge, "Shape sensing using multi-core fiber optic cable and parametric curve solutions," Opt. Express **20**(3), 2967–2973 (2012).
14. M. N. Alahbabi, N. P. Lawrence, Y. T. Cho, and T. P. Newson, "High spatial resolution microwave detection system for Brillouin-based distributed temperature and strain sensors," Meas. Sci. Technol. **15**(8), 1539–1543 (2004).
15. S. M. Maughan, H. H. Kee, and T. P. Newson, "Simultaneous distributed fibre temperature and strain sensor using microwave coherent detection of spontaneous Brillouin backscatter," Meas. Sci. Technol. **12**(7), 834–842 (2001).